Poroelastic Modelling of Production and Injection-Induced Stress Changes in a Pinnacle Reef

H. Soltanzadeh & C.D. Hawkes
University of Saskatchewan, Saskatchewan, Canada

P.J. McLellan
Weatherford Advanced Geotechnology, Calgary, Alberta, Canada

S.A. Smith
Energy & Environmental Research Center (EERC), Grand Forks, ND, USA

ABSTRACT: This paper summarizes semi-analytical and closed-form solutions that can be used to assess the poroelastic stress changes induced within a porous formation (reservoir) during a pore pressure change. Further, solutions are presented for the stress discontinuities at the interfaces between reservoirs and the rocks that surround them. When used in combination with rock failure criteria, these solutions enable relatively simple analyses of the potential for induced fracturing or fault reactivation within a reservoir or the rock immediately adjacent to it. The latter, in particular, is useful for assessing if the hydraulic integrity of the surrounding rock (i.e., the bounding seal) will be affected by a pore pressure change. The use of the approach presented in this paper is illustrated with an analysis of a pinnacle reef with dimensions and properties representative of reefs in the Zama oil field, northwestern Alberta, Canada. Scenarios of pore pressure decrease (during historical production operations) and pore pressure increase (during several years of acid gas injection operations) are analyzed, for three different idealizations of reservoir properties and geometry (two plane strain and one axisymmetric). These results suggest that that the potential for induced fracturing is not significant at any point within the reservoir or the surrounding rock for both the production and injection scenarios that were simulated. Similarly, fault reactivation was not predicted for the reservoir or any of the points that were analyzed in the surrounding rock. However, fault orientations having the greatest potential for reactivating during historical production operations were identified; thus, illustrating a means of using geomechanical models to focus geological characterization efforts on the features that are most critical to acid gas containment.

1 INTRODUCTION

During fluid production from hydrocarbon reservoirs, and fluid injection for enhanced oil recovery, greenhouse gas sequestration or waste disposal, stress changes are induced within and surrounding the reservoir. To ensure that production or injection can be maintained in a safe and effective manner, it is necessary to assess the effect of these stress changes on the hydraulic integrity of the rocks that bound the reservoir. For example, if shear or tensile fractures are induced, or if existing faults or fractures are re-opened or reactivated, these features are likely to serve as fluid leakage paths. Geomechanical models that can be used to assess the potential for creating (or enhancing) such leakage paths include closed-form (or analytical) solutions, semi-analytical solutions and numerical models. The first two types, due to their relatively modest computational requirements, are useful for preliminary modelling, for analyzing parameter sensitivies, and for probabilistic simulations. The latter type is useful for its ability to model more complex material behaviours and reservoir geometries. In many projects, a logical sequence is to start with closed-form and/or semi-analytical models to identify potential leakage hazards, then progress to numerical modelling to develop a refined understanding of these hazards.

This paper begins by presenting a summary of closed-form and semi-analytical models that are appropriate for geomechanical modelling of induced fracturing and fault/fracture reactivation potential in a reservoir that has undergone a historical pore pressure reduction due to fluid withdrawal, followed by pore pressure increase due to fluid injection. The application of some of these solutions is then illustrated for a pinnacle reef with properties representative of the reefs present in the Zama oil field of northwest Alberta, Canada, which is currently an acid gas injection site.

2 INDUCED STRESS ANALYSIS USING SEMI-ANALYTICAL MODELS

Semi-analytical models for stress change induced by pressure and temperature change have been developed using three different theories of elasticity (for more details see Soltanzadeh and Hawkes, 2009): (i) the theory of strain nuclei (e.g., Segall 1985; Segall et al, 1994); (ii) the theory of inclusions (e.g., Segall and Fitzgerald, 1998; Soltanzadeh and Hawkes, 2008); and (iii) the theory of inhomogeneities (e.g., Rudnicki, 1999; Soltanzadeh et al., 2007). [Note: This paper will focus on pore pressure-induced stress changes, though the analysis of temperature-induced changes could readily be conducted in an analogous manner.] In models based on these theories, induced stress changes can be linearly related to the pore pressure change within the reservoir. Soltanzadeh and Hawkes (2009) defined normalized stress arching ratios based on this linear relationship as follows:

$$\gamma_{\alpha(H_1)} = \Delta\sigma_{H_1} /(\alpha\Delta P)\,,\ \gamma_{\alpha(H_2)} = \Delta\sigma_{H_2} /(\alpha\Delta P)\,, \gamma_{\alpha(V)} = \Delta\sigma_{V} /(\alpha\Delta P) \quad (1)$$

where $\gamma_{\alpha(H1)}$, $\gamma_{\alpha(H2)}$ are normalized horizontal stress arching ratios (in two perpendicular directions); $\gamma_{\alpha(V)}$ is the vertical stress arching ratio; $\Delta\sigma_{H1}$, $\Delta\sigma_{H2}$, and $\Delta\sigma_{V}$, respectively, are the corresponding horizontal and vertical stress changes; α is Biot's coefficient; and ΔP is the reservoir's pore pressure change (which, in this paper, is approximated as being uniform throughout the reservoir). Assuming that the stress arching ratios for a given reservoir have been determined, the effective stress change within the reservoir can be calculated as follows:

$$\Delta\sigma'_{H1} = -(1-\gamma_{\alpha(H1)})(\alpha\Delta P) \quad (2a)$$

$$\Delta\sigma'_{H2} = -(1-\gamma_{\alpha(H2)})(\alpha\Delta P) \quad (2b)$$

$$\Delta\sigma'_{V} = -(1-\gamma_{\alpha(V)})(\alpha\Delta P) \quad (2c)$$

and because it has been assumed that no pressure change occurs in the surrounding rock, effective stress change in this region can be found as:

$$\Delta\sigma'_{H1} = \gamma_{\alpha(H1)}(\alpha\Delta P) \quad (3a)$$

$$\Delta\sigma'_{H2} = \gamma_{\alpha(H2)}(\alpha\Delta P) \quad (3b)$$

$$\Delta\sigma'_{V} = \gamma_{\alpha(V)}(\alpha\Delta P) \quad (3c)$$

Values of arching ratios can be determined using any of the aforementioned theories. Soltanzadeh and Hawkes (2008) developed a semi-analytical solution based on theory of inclusions for a reservoir in a plane-strain half-space. Limitations of this solution include the fact that it presumes the reservoir to be (strictly-speaking) infinitely long in one horizontal direction, have constant shape (elliptical, in this case) and dimensions in the plane normal to this direction, and possess elastic properties that are uniform and identical to those of the surrounding rock. A strength of this solution is the fact that it can account for the effect of a free surface (i.e., ground surface) at some finite elevation above the reservoir. Soltanzadeh and Hawkes (2008) showed that stress arching ratios for such a reservoir are functions of two dimensionless geometrical parameters; reservoir aspect ratio (*e*) and depth number (*n*):

$$e = T / W \ ; \ n = W / (2D) \tag{4}$$

where *T* is the reservoir's maximum thickness, *W* is the reservoir's width, and *D* is the depth of reservoir's central point. Based on the studies by Soltanzadeh and Hawkes (2008), the effect of the free surface on the geomechanical response of the reservoir is negligible if the depth number is very small (i.e., $n < 0.1$). In addition, the effect of depth is insignificant for thin reservoirs (i.e., $e < 0.2$) for depth numbers less than 0.5. Therefore, for cases that meet these conditions, it is possible to use solutions based on a plane-strain full-space geometry (i.e., the effects of ground surface are neglected) with sufficient accuracy. Fortunately, in a full-space, closed-form solutions can be derived using the theories of inclusions and inhomogenitoes to calculate arching ratios within reservoirs with idealized geometries. Soltanzadeh and Hawkes (2009) presented a number of such solutions for different geometric variations of ellipsoidal reservoirs. For instance, for a cylindrical reservoir with an elliptical cross-section, arching ratios within the reservoir are (Soltanzadeh and Hawkes, 2009):

$$\gamma_{\alpha(H_1)} = \frac{1-2\nu}{1-\nu}\frac{1}{1+e}; \quad \gamma_{\alpha(H_2)} = \frac{1-2\nu}{1-\nu}; \quad \gamma_{\alpha(V)} = \frac{1-2\nu}{1-\nu}\frac{e}{1+e} \tag{5}$$

where ν is Poisson's ratio of the reservoir and the surrounding rock. The index H_1 denotes the horizontal direction in the cross-sectional plane (i.e., the in-plane component), and H_2 denotes the horizontal direction parallel to the reservoir's axis (i.e., the out-of-plane component). Also, for an oblate spheroid (i.e., an axisymmetric ellipsoid with aspect ratio (*e*) less than one) with a vertical axis of symmetry, the poroelastic normalized stress arching ratios are (Fjaer et al., 2008, p. 397; Soltanzadeh and Hawkes, 2009):

$$\begin{aligned} \gamma_{\alpha(H_1)} = \gamma_{\alpha(H_2)} &= \frac{1}{2}\frac{1-2\nu}{1-\nu}\left[1 + \frac{1}{1-e^2} - \frac{e\cos^{-1}e}{(1-e^2)^{3/2}}\right] \\ \gamma_{\alpha(V)} &= \frac{1-2\nu}{1-\nu}\left[\frac{e\cos^{-1}e}{(1-e^2)^{3/2}} - \frac{e^2}{1-e^2}\right] \end{aligned} \tag{6}$$

Although numerical integration can be used to semi-analytically calculate stress arching ratios at all points in the surrounding rock, it is possible to use the concept of discontinuities to calculate these parameters at those points in the surrounding rock that are adjacent to the reservoir. Based on this concept, in a homogenous field, there is a constant discontinuity in the tangential direction as follows (e.g., Segall and Fitzgerald, 1998):

$$\gamma_{\alpha(Tangantinal)}\Big|_{Reservoir} - \gamma_{\alpha(Tangantinal)}\Big|_{Surrounding} = \frac{1-2\nu}{1-\nu} \tag{7}$$

Further, the normal stresses at the both sides of the interface (i.e., within reservoir and in surrounding rock) are identical.

When there is a contrast between elastic properties of the reservoir and surrounding rock, the theory of inhomogeneities can be implemented to calculate stress arching ratios for a full-space field embedding an ellipsoidal reservoir. Soltanzadeh and Hawkes (2009) derived closed-form solutions to calculate arching ratios within different variations of an ellipsoidal reservoir geometry. Their solution for a very long reservoir with an elliptical cross section (i.e., plane strain solution) was as follows:

$$\gamma_{\alpha(H_1)} = A_1 / A_4 \ ; \ \gamma_{\alpha(H_2)} = A_2 / A_4 \ ; \ \gamma_{\alpha(V)} = A_3 / A_4 \tag{8}$$

where,

$$A_1 = (1-2\nu^*)[R_\mu[e(1-2\nu)+2(1-\nu)]+e] \tag{9a}$$

$$A_2 = (1-2\nu^*)[R_\mu[R_\mu e(3-4\nu)+2(1+e^2)(1-\nu)]+e] \tag{9b}$$

$$A_3 = (1-2\nu^*)[R_\mu[2e(1-\nu)+1-2\nu]+1]e \tag{9c}$$

$$\begin{aligned} A_4 = {} & R_\mu[2(1+e)^2(1-\nu)(1-\nu^*)-2e\nu^*(1-2\nu)+R_\mu e(3-4\nu)] \\ & +e(1-2\nu^*) \end{aligned} \tag{9d}$$

where ν and ν^* are Poisson's ratios of the surrounding rock and reservoir, respectively, and R_μ is shear modulus ratio; i.e., the ratio of shear modulus within reservoir (μ^*) to shear modulus in surrounding rock (μ).

Stress arching ratio discontinuities for points in the surrounding rock, adjacent to the reservoir, were presented by Soltanazadeh et al. (2007) as follows:

$$Dis(\gamma_{\alpha(H_1)}) = \frac{2}{1-\nu}\varepsilon^{**}_{N(H)} \ ; \ Dis(\gamma_{\alpha(V)}) = \frac{2}{1-\nu}\varepsilon^{**}_{N(V)} \tag{10}$$

Where $\varepsilon^{**}_{N(H)}$ and $\varepsilon^{**}_{N(V)}$, respectively, are normalized fictitious horizontal and vertical strains and can be written as:

$$\varepsilon^{**}_{N(H1)} = \frac{B_1}{A_4} \ , \ \varepsilon^{**}_{N(V)} = \frac{B_2}{A_4} \tag{11}$$

where:

$$B_1 = [R_\mu[(1+e)^2(1-\nu)-e^2]+e^2](1-2\nu^*)(1-\nu) \tag{12a}$$

$$B_2 = [R_\mu[(1+e)^2(1-\nu)-1]+1](1-2\nu^*)(1-\nu) \tag{12b}$$

[Note: At the time this paper was written, the authors were unaware of any closed-form solutions for stress arching ratio discontinuities around the boundaries of axisymmetric, ellipsoidal reservoir geometries using the theory of inhomogeneities (i.e., accounting for elastic property contrast between the reservoir and surrounding rock).]

Following, a case study is used to demonstrate the application of these closed-form solutions to induced stress-change analysis at an acid gas injection site. Based on the stress changes, the potential for tensile fracturing is assessed, as well as the potential for fault reactivation and induced shear fracturing in the reservoir and the rock immediately surrounding it.

3 CASE STUDY: ACID GAS INJECTION IN THE ZAMA OIL FIELD

The Zama oil field is located in northwestern Alberta, Canada, and covers an area of 1200 km^2. The field contains more than 400 pinnacle reefs of the Middle Devonian Keg River Formation. Injection of a stream of acid gas (approximately 70% CO_2 and 30% H_2S) started in December 2006. To date, injection has occurred in four pinnacles; the goal is to inject into several more pinnacles in the coming years. In this paper, the effects of geomechanical processes on the hydraulic integrity of a single, representative pinnacle reef is investigated. For the case considered, the reservoir consists of dolomite of varying porosity and permeability. In reality, it is overlain and laterally bounded by anhydrites of the Muskeg Formation, and underlain by lower-porosity carbonates of the Keg River Formation. For the purposes of this work, the reservoir will be analyzed as if it were completely surrounded by the Muskeg Formation. The effects of historical pressure depletion due to oil production will be considered in this work, as well as future pressure increases due to fluid injection (waterflooding conducted mid-life in the reservoir's history, and more recently acid gas injection).

3.1 *Reservoir geometry*

The actual reservoir shape to be analyzed is a pinnacle (see Figure 1) of 90 m height and 0.16 km^2 base area, at a mid-point depth of 1500 m. To enable the use of the closed-form solutions presented earlier in this paper, the reservoir shape has been simplified to an axisymmetric spheroid with the same height and volume of the reservoir; this gives a reservoir width of 320 m. [Note: This same reservoir width has been used in all of the analyses that follow, even though the concept of reservoir volume is ill-defined in the case of plane-strain (i.e., infinitely long) reservoir geometries.] As such, the idealized reservoir has the following geometrical characteristics:

- aspect ratio, e = 90/320 = 0.28
- depth number, n = (320/2) / 1500 = 0.11

Based on a comparison of these geometrical parameters with the criteria presented in Section 2 of this paper, full-space solutions can be used for this reservoir without incurring significant error.

3.2 *In-situ stresses and pressure history*

Bachu at al. (2008) estimated values of 17 and 24 kPa/m, respectively, for typical minimum horizontal and vertical stress gradients in the Keg River formation in Zama field. Bell and Babcock (1986) believe that the ratio of maximum to minimum horizontal stress in Western Canadian Basin varies between 1.3 to 1.6. A value of 1.4 was used in this specific case, which leads to a value o 24 kPa/m for the gradient of maximum horizontal stress. As such, the stress regime interpreted for this site is transitional between strike-slip and normal.

An initial reservoir pressure of 14.5 MPa was used for this site. During primary production, pressure decreases to slightly less than 4 MPa. During injection, pore pressure will remain lower than the minimum in-situ stress in the caprock, which – based on the information presented above - is the minimum horizontal stress. Its magnitude is estimated as 17 kPa/m × 1500 m = 25.5 MPa. For the sake of working in round numbers, pore pressure change scenarios of ± 10 MPa are considered in this paper.

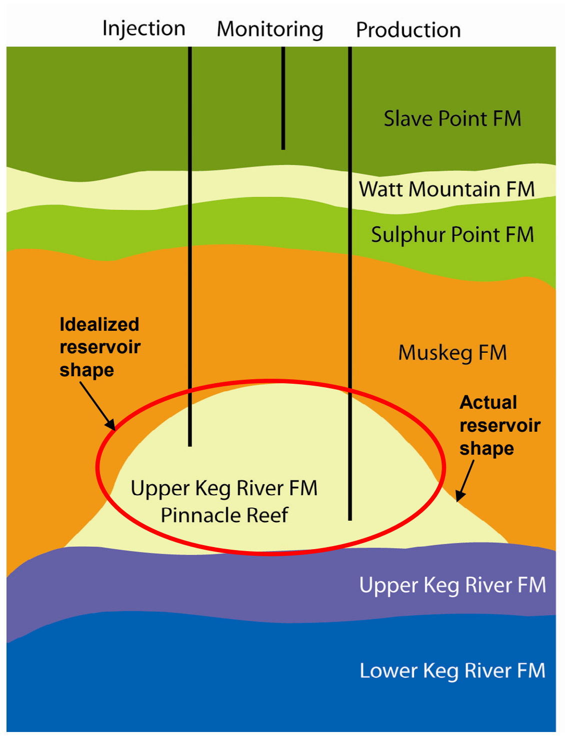

Figure 1. Schematic of actual and idealized reservoir geometry (after Smith et al., 2008)

3.3 *Rock mechanical properties*

Based on geophysical log analysis and laboratory testing on core samples, mechanical properties of the Keg River Formation reservoir rocks and the "surrounding" Muskeg Formation anhydrite were reported by Smith et al. (2008). Table 1 lists the mechanical properties selected for use in this paper. Based on these values, the shear modulus ratio ($R_\mu = \mu^*/\mu$) is calculated as 0.46. It is worthy to note that Poisson's ratio of the surrounding rock does not have a significant effect on the stress change induced by pressure change (Rudnicki, 1999; Soltanzadeh and Hawkes, 2008). Peak strength properties in Table 1 (e.g., friction angle and cohesion) are used in this paper to evaluate the onset of shear fracturing. Residual friction angle is used as a friction angle on potentially existing faults in the field. A Biot's coefficient of 1.0 was used for both the Keg River and Muskeg formations.

Table 1. Rock mechanical properties for a representative pinnacle reef in the Zama oil field.

Geomechancial properties	Reservoir (Keg River Formation)	Surrounding rock (Muskeg Formation)
Static shear modulus (μ)	11 GPa	24 GPa
Static Poisson's ratio (ν)	0.23	0.26
Peak friction angle (ϕ_p)	37°	53°
Peak cohesion (c_p)	4 MPa	12 MPa
Residual friction angle (ϕ_r)	34°	44°
Residual cohesion (c_r)	2.2 MPa	6.5 MPa
Permeability (k)	95–175 mD	
Porosity (ϕ)	12%	2%

3.4 *Induced stress change analysis*

Equations (5) to (12) were used to calculate the normalized stress arching ratios for production (pressure depletion) and injection (pressure increase) for three different reservoir scenarios: (i) a plane strain elliptical inclusion, analyzed in a cross-sectional plane aligned parallel to the minimum horizontal stress; (ii) a plane strain elliptical inhomogeneity, also analyzed in a cross-sectional plane aligned parallel to the minimum horizontal stress; and (iii) an axisymmetric inclusion. These arching ratios were then used with equations (1) and (2) to calculate induced stress changes in the field at the following locations: (i) within the reservoir; (ii) at a point in the caprock immediately overlying the centre of the reservoir (referred to as "caprock" in the following discussion and figures); (iii) at a point in the caprock immediately adjacent to the side of the reservoir in the cross-sectional plane (referred to as the "sideburden, in the σ_{Hmin} direction" in the following discussion and figures); and (iv) at a point "in front of" the reservoir; i.e., in the surrounding rock immediately adjacent to the side of the reservoir in the out-of-plane direction (referred to as the "sideburden, in the σ_{Hmax} direction"). [Note: The latter point is only applicable for the axisymmetric case.]

The total stress changes calculated for the aforementioned locations for a pore pressure increase of 10 MPa (ΔP = 10 MPa) are shown in Table 2. Due to the linear elastic nature of the solutions used, the stress changes for a depletion scenario (ΔP = -10 MPa) would be identical to those listed in Table 2, multiplied by -1. Figures 2 and 3 show both total and effective in-situ stress states before and after a 10 MPa pore pressure change for a production scenario and an injection scenario, respectively. Using these figures or Table 2, it can be seen that, during injection, the following stress changes occur:

- Within the reservoir, all stress changes are tensile.
- In the caprock, in-plane horizontal stress change is tensile; vertical stress change is compressive; out-of-plane horizontal stress change varies for the different scenarios.
- In the sideburden (σ_{Hmin} direction), in-plane horizontal stress change is compressive; vertical stress change is tensile; out-of-plane horizontal stress change is either zero (plane-strain inclusion) or tensile.
- In the sideburden (σ_{Hmax} direction – axisymmetric case only), in-plane horizontal stress change is tensile; vertical stress change is tensile; out-of-plane horizontal stress change compressive.

Conceptually, all of these stress changes can be understood on the grounds that, during injection, the reservoir is expanding; hence, pushing outwards on the surrounding rock. For the pressure depletion case, in which the reservoir is contracting, the stress changes are exactly opposite to those summarized above.

One final point worth noting is the fact that the vertical stress increase predicted in the sideburden is markedly larger for the plane-strain inhomogeneity case compared to both of the inclusion cases, which are similar in magnitude. This is a consequence of the fact that, for the former case, the surrounding rock is stiffer than the reservoir. As the latter presses outwards (during injection), this induces a large stress in the sideburden in the direction that is tangential to the reservoir – host rock interface (i.e., the vertical direction).

3.5 *Failure analysis*

Analyses of induced shear fracturing and fault reactivation are described in this section of the paper. [Note: For simplicity, the term fault will be used in this section to refer to any discontinuity, including faults, natural fractures and joints.] Although these analyses could be conducted with any of the induced stress change models described in the previous section, the axisymmetric solution based on the theory of inclusions has been selected for use in this paper; although it neglects the effects of material property contrasts, it better captures the actual reservoir geometry.

Peak strength properties in Table 1 were used for induced shear fracturing analysis, and residual friction angles were used to calculate the friction coefficients of faults or natural fractures, which were assumed to have no cohesive strength. Given that no data are available on the presence of, nor the orientation of, faults or natural fractures, the conservative assumption of "critically oriented" faults or fractures was used; i.e., reactivation was assessed for hypothetical faults or fractures that are oriented such that they are most likely to fail.

The stress states calculated before and after reservoir pressure change are presented using Mohr circles in Figures 4 and 5 for production (pressure depletion) and injection, respectively. These figures show that:

1) Within the reservoir:
   a. During production, though the increase of effective stresses moves the stress state away from both the intact rock and fault failure criteria, the increase in deviatoric stress partially opposes this beneficial effect. Ultimately, the net effect is such that the stress state would have shifted toward a more stable condition during historical production operations (Figure 4a).
   b. During injection, the stress state is predicted to become more critical; i.e., the stress state shifts towards the fault and intact rock failure criteria (Figure 5a). Although this suggests an increased potential for failure in a relative sense, it is significant to note that neither of these failure criteria is met in an absolute sense.
2) In the sideburden aligned with the minimum horizontal stress (i.e., σ_{Hmin} direction):
   a. During production, due to the increase in vertical stress and maximum horizontal stress and the decrease in minimum horizontal stress, the stress state becomes more deviatoric. As such, during production the stress state may have come close to meeting the failure criterion for optimally oriented faults (or natural fractures), *if* any were present (Figure 4b). In this case, the "most" optimally oriented faults would have steep dips (~60°) and strike directions sub-parallel to the maximum horizontal stress azimuth; however, sub-vertical faults striking at acute angles (~30°) to the maximum horizontal stress would be only "slightly less" optimally

Table 2. Calculated stress changes for a 10 MPa pore pressure increase.

Location	**Stress change compo-nent**	**Stress change (MPa)**		
		Plane strain inclusion	**Plane strain inhomogeneity**	**Axisymmetric inclusion (oblate spheroid)**
Within reservoir	$\Delta\sigma_H$	7	7.6	5.9
	$\Delta\sigma_h$	5.5	6.9	5.9
	$\Delta\sigma_V$	1.5	2.7	2.3
Caprock	$\Delta\sigma_H$	0	0.4	-1.1
	$\Delta\sigma_h$	-1.5	-1.2	-1.1
	$\Delta\sigma_V$	1.5	2.7	2.3
Sideburden (in the σ_{Hmin} Direction)	$\Delta\sigma_H$	0	-1.4	-1.1
	$\Delta\sigma_h$	5.5	6.9	5.9
	$\Delta\sigma_V$	-5.5	-12.5	-4.7
Sideburden (in the σ_{Hmax} direction)	$\Delta\sigma_H$	N/A	N/A	5.9
	$\Delta\sigma_h$	N/A	N/A	-1.1
	$\Delta\sigma_V$	N/A	N/A	-4.7

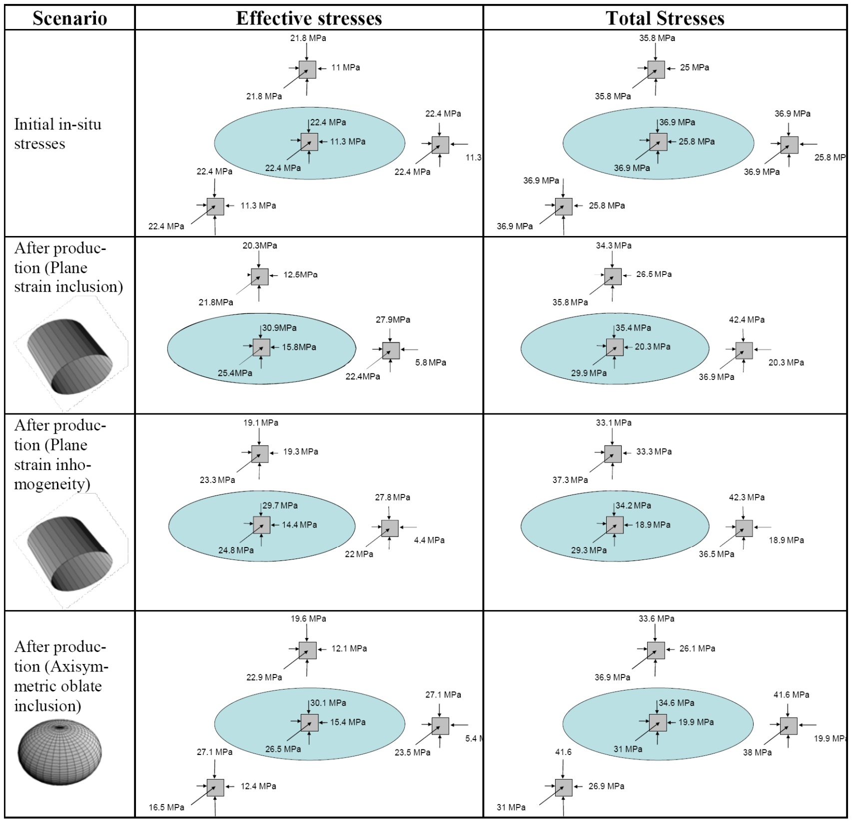

Figure 2. Total and effective stresses before and after pressure depletion of 10 MPa, calculated for different reservoir scenarios.

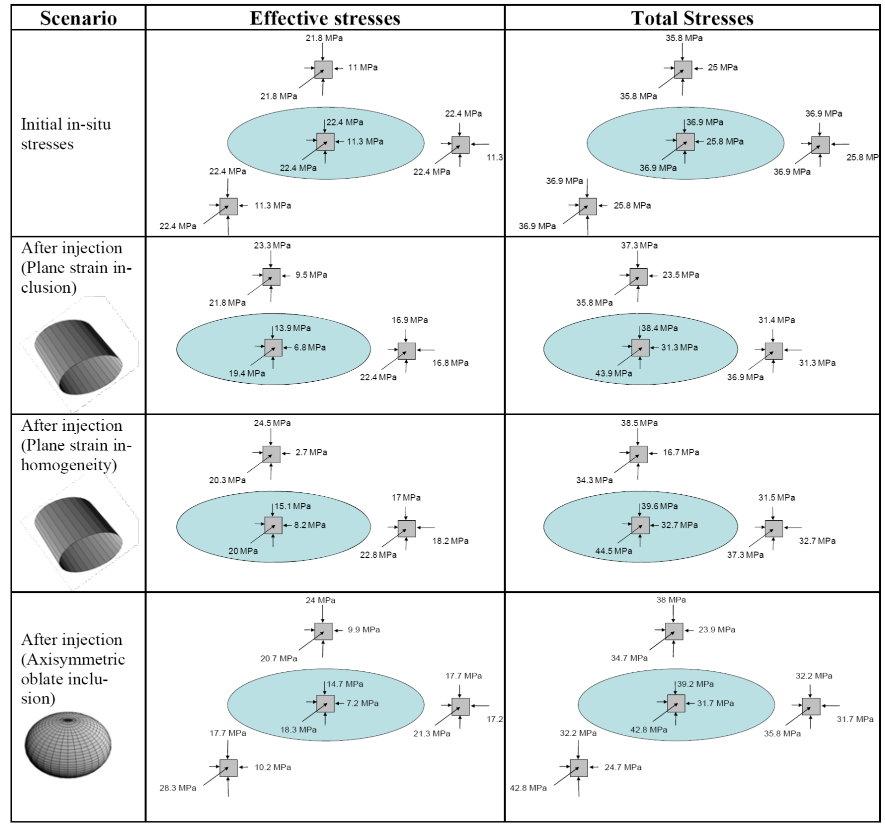

Figure 3. Total and effective stresses before and after 10 MPa pressure increase due to injection, calculated for different reservoir scenarios.

oriented. As for induced fracturing, given the high strength of the Muskeg Formation (i.e., the failure criterion is barely visible in the top left corner of the graph), the stress state during production is not likely to have induced new shear fractures.

   b. During injection, due to the decrease in vertical stress and maximum horizontal stress and the increase in minimum horizontal stress, the stress state is predicted to become more isotropic, leading to a more stable rock condition (Figure 5b).

3) In the sideburden aligned with maximum horizontal stress (i.e., σ_{Hmax} direction):
   a. During production, minimal change in the potential for fault reactivation or induced fracturing is likely to have occurred (Figure 4c).
   b. During injection, although vertical stress decreases, the increase in maximum horizontal stress and the decrease in minimum horizontal stress results in an increase in the deviatoric stress in the horizontal plane. As shown in Figure 5c, this results in a modest increase in the potential for failure.
4) In the caprock:
   a. During production, minimal change (a slight reduction, in fact) in the potential for fault reactivation or induced fracturing is likely to have occurred (Figure 4d).
   b. During injection, due to the increase in vertical stress and the decrease in horizontal stresses, the deviatoric stresses increases. As such, the stress state would become slightly more critical, but still quite far from failure in an absolute sense (Figure 5d).

The effective stress state did not approach a tensile condition for any of the scenarios analyzed; i.e., the potential for induced tensile fracturing within and surrounding the reservoir is predicted to be low for these scenarios.

4 CONCLUSION

Closed-form solutions based on the theories of inclusions and inhomogeneities have been presented, which can be used to calculate induced stress change within a reservoir during pore pressure change. Using the concept of stress arching ratio discontinuities at the interface between the reservoir and the surrounding rock, induced stress changes can be calculated in the rocks adjacent to the reservoir.

The use of these solutions has been illustrated with an analysis of induced stress changes due to historical oil production, with resultant pore pressure depletion, and pore pressure increases resulting from waterflooding and/or acid gas injection in a pinnacle reef in the Zama oil field, Alberta. The results generated are consistent with the expectation that, during injection, the reservoir is expanding; hence, pushing outwards on the surrounding rock. This results in a compressive stress change in directions oriented normal to the reservoir-host rock interface, and a tensile stress change in direction tangential to the interface. The results generated for a plane-strain reservoir geometry, in which the high stiffness of the host rock relative to the reservoir was accounted for, demonstrate that this contrast can significantly increase some of the stress change magnitudes. During pressure depletion, the stress changes are exactly opposite to those described for injection.

Failure analyses for both the fault reactivation and induced fracturing were performed, using the stress changes predicted for an axisymmetric ellipsoidal reservoir geometry. These analyses showed that the potential to induce shear fracturing was not significant at any point within the reservoir or the surrounding rock during both production and injection. Similarly, fault reactivation was not predicted for the reservoir or any of the points that were analyzed in the surrounding rock. However, fault orientations at points in the sideburden having the greatest potential for reactivating during historical production operations were identified. This illustrates a means of using geomechanical models to focus geological characterization efforts on the features that are most critical to acid gas containment.

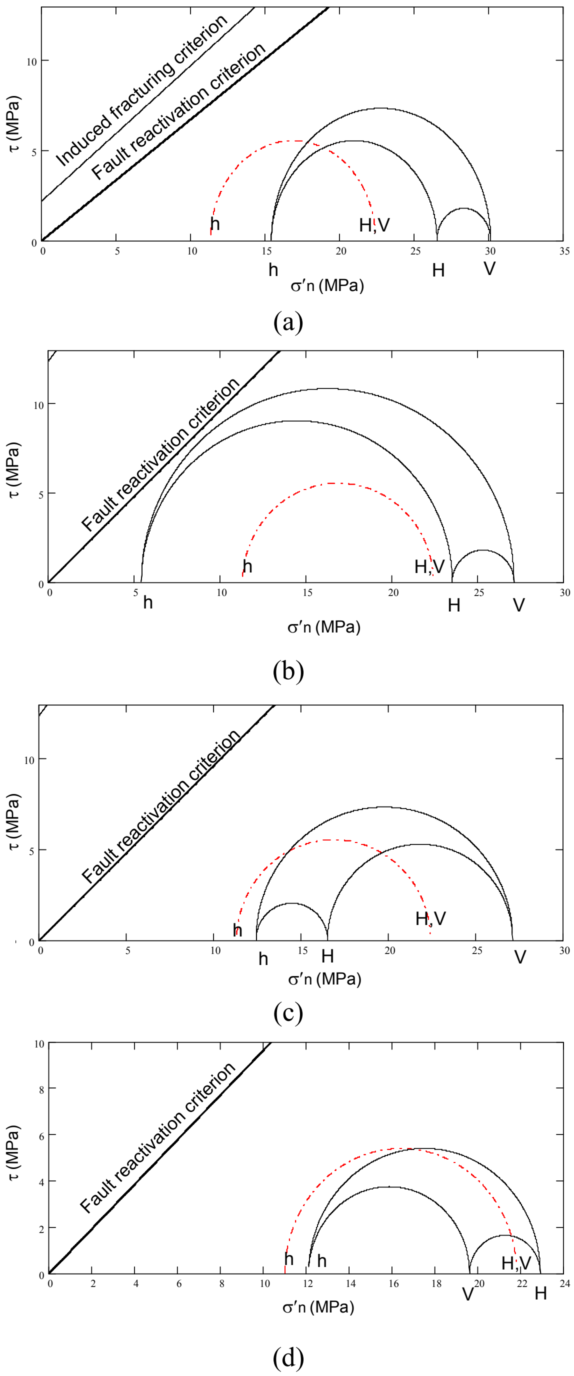

Figure 4. Effective stress state after pressure depletion of 10 MPa: (a) within the reservoir; (b) in the sideburden aligned with minimum horizontal stress; (c) in the sideburden aligned with maximum horizontal stress; and (d) in the caprock. The dashed circle represents the original stress state, in which the maximum horizontal stress and the vertical stress magnitudes are equal. H denotes the maximum horizontal stress, h denotes the minimum horizontal stress, and V denotes the vertical stress.

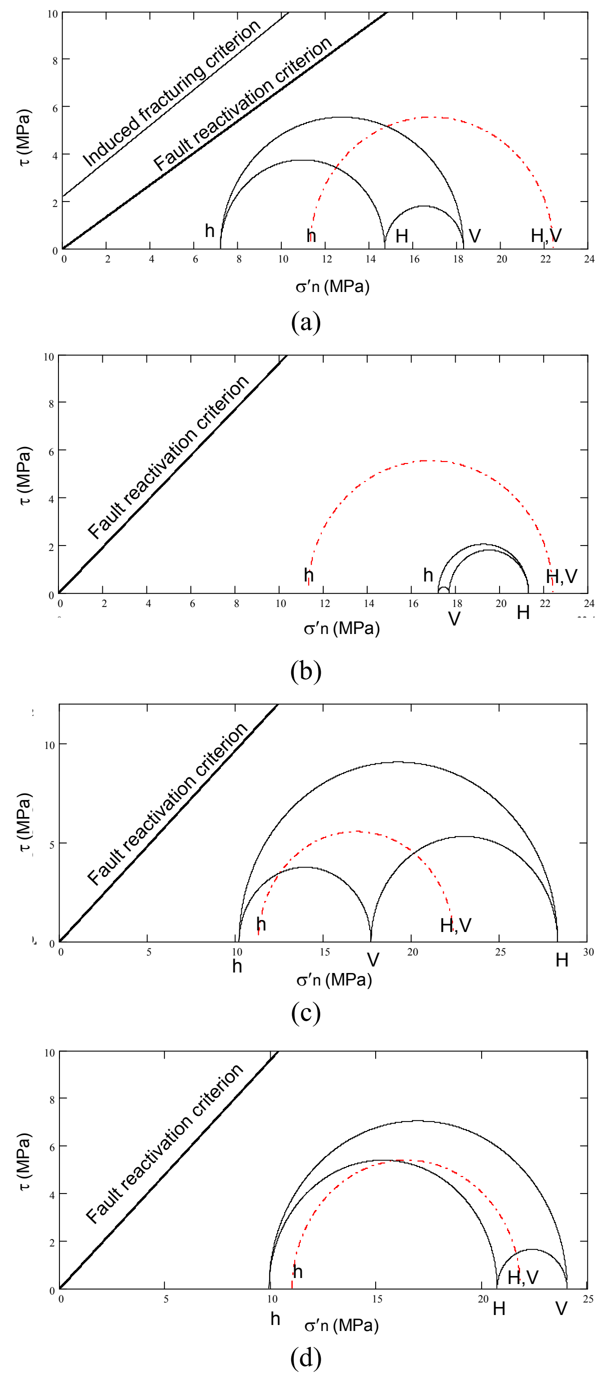

Figure 5. Effective stress state after a pressure increase of 10 MPa: (a) within the reservoir; (b) in the sideburden aligned with minimum horizontal stress; (c) in the sideburden aligned with maximum horizontal stress; and (d) in the caprock. The dashed circle represents the original stress state, in which the maximum horizontal stress and the vertical stress magnitudes are equal. H denotes the maximum horizontal stress, h denotes the minimum horizontal stress, and V denotes the vertical stress.

5 REFERENCES:

Bachu S., Haug K., and Michael K. 2008. Stress Regime at Acid-Gas Injection Operations in Western Canada. *ERCB/AGS Special Report 094 (March).*

Bell J.S., and Babcock E.A. 1986. The stress regime of the Western Canadian basin and implications for hydrocarbon production, *Bulletin of Canadian Petroleum Geology*, 34: 364–378.

Fjaer E., Holt R.M., Horsrud P., Raaen A.M., and Risnes R. 2008. *Petroleum Related Rock Mechanics, 2nd Edition*. Elsevier, Amsterdam.

Rudnicki, J.W. 1999. Alteration of regional stress by reservoirs and other inhomogeneities: stabilizing or destabilizing? *Proc. 9th Int. Congress on Rock Mechanics*, Paris, France, Swets & Zeitlinger: Lisse, Netherlands, 3:1629-1637.

Segall, P. 1985. Stress and subsidence resulting from subsurface fluid withdrawal in the epicentral region of 1983 Coalinga earthquake. *Journal of Geophysical Research*, 90: 6801-6816.

Segall, P.; Fitzgerald, S.D. 1998. A note on induced stress change in hydrocarbon and geothermal reservoirs. *Tectonophysics*, 289: 117-128.

Segall, P.; Grasso, J.R.; Mossop, 1994. A. Poroelastic stressing and induced seismicity near the Lacq gas field, southwestern France. *Journal of Geophysical Research*, 99(B8): 15423–15438.

Smith S.A., McLellan P., Hawkes C.D., Steadman E.N., and Harju J.A. 2008, Geomechanical Testing and Modeling of Reservoir and Cap Rock Integrity in an Acid Gas EOR/Sequestration Project, Zama, Alberta, Canada. *Poster presented at the 9th International Conference on Greenhouse Gas Control Technologies, November 16 – 20, 2008, Washington DC.*

Smith S.A., Sorensen J.A., Steadman E.N., Harju J.A., Jackson W.A., Nimchuk D., and Lavoie, R. 2007. Zama Acid Gas EOR, CO2 Sequestration and Monitoring Project. *Sixth Annual Conference on Carbon Capture & Sequestration, Pittsburgh, PA, USA, May 7, 2007.*

Soltanzadeh H., and Hawkes C.D. 2008. Semi-Analytical Models for Stress Change and Fault Reactivation Induced by Reservoir Production and Injection, *Journal of Petroleum Science and Engineering*, 60(2): 71-85.

Soltanzadeh H., and Hawkes C.D. 2009. Induced Poroelastic and thermoelastic stress changes within reservoirs during fluid injection and production, *Porous Media: Heat and Mass Transfer, Transport and Mechanics* (Chapter 2), Hauppauge, NY, USA, Nova Science Publishers, Inc.,

Soltanzadeh, H.; Hawkes, C.D.; Sharma, J. 2007. Closed-form solutions for production- and injection-induced stresses in plane-strain reservoirs with elastic properties different from the surrounding rock, *International Journal of Geomechanics*. 7(5): 353-361.